An NFC-Connected Coupler Using IPT-CPT-Combined Wireless Charging for Metal-Cover Smartphone Applications

Jia-Qi Zhu, Yong-Ling Ban, Rui-Min Xu, *Member, IEEE*, and Chunting Chris Mi, *Fellow, IEEE*

***Abstract*—A near field communication (NFC)-connected coupler using inductive power transfer (IPT)-capacitive power transfer (CPT)-combined wireless charging is proposed for metal-cover smartphone applications. To mitigate eddy current loss in the metal cover, CPT is introduced. Compared with traditional CPT, wireless power transfer through a metal cover is realized, and cost and valuable space inside the smartphone are saved. To achieve CPT through a metal cover, the metal cover itself is separated by a cross slot and utilized as receiving plates. To reduce the voltage across the metal cover within a safety range, IPT is applied. The already-existing NFC antenna is first used as the receiving coil for IPT and also performs as the compensated inductance for CPT. By connecting one of its feed lines to the metal cover, only a parallel external capacitor is needed to construct the receiver of the proposed coupler because the metal cover and NFC antenna are components that already exist inside the smartphone, which greatly saves space inside the smartphone and cost for the proposed coupler. Prototypes of the proposed NFC-connected coupler with and without actual smartphone have been built. The wireless power transfer through metal cover by IPT and CPT has been validated via experiment.**

***Index Terms*—Capacitive power transfer (CPT), inductive power transfer (IPT), metal cover, near field communication (NFC), smartphone application.**

I. Introduction

WIRELESS power transfer (WPT) is a user-friendly charging technology for consumer electronic devices, which utilizes electromagnetic field to transfer power without an electric contact [1]. In recent years, with the rapid expansion of the smartphone market, integrating a WPT coupler into a mobile handset is now becoming a necessity due to its advantages of being cordless, waterproof and user friendly over a conventional plug-in charger [2]. With regard to nonmetallic-cover smartphones, inductive power transfer (IPT) is widely applied with Qi standard [3]–[5]. However, for metal-cover smartphones, eddy current will be induced and the magnetic field lines will be blocked by the metal cover, resulting in low power and efficiency [6], [7]. In this case, capacitive power transfer (CPT) is a good alternative because the electric field generated by the capacitive coupler does not induce significant eddy-current loss in nearby metal objects [8]–[10]. Since two separate metal plates are needed for a receiving capacitive coupler, the metal cover itself can be utilized as receiving plates and no metal barrier is sandwiched between the transmitter and receiver. Here, people may touch the metal cover during the charging process so that the voltage on the metal cover needs to be constrained within a safety range, which is 8.35 V for high frequency (HF) applications [11]–[13]. Nevertheless, if only capacitive charging is applied, it is hard to limit the voltage on the metal cover within a safety range because the CPT capability is in proportion to the voltage across the metal plates. In this circumstance, if both IPT and CPT are applied to transfer power, eddy current loss can be mitigated and voltage on the metal cover can be reduced within a safety range. Besides, an IPT-CPT-combined coupler can significantly save valuable space inside a compact smartphone because the inductive coil of IPT can also be utilized as the compensation inductance for CPT and vice versa. Above all, IPT-CPT-combined wireless charging is a promising technology for metal-cover smartphones.

Both inductive and capacitive couplers can be classified by circuit topology. The inductive coupler can be classified as series-none (SN) topology [14], double-sided series or parallel topology (series–series, series–parallel, parallel–series, and parallel–parallel) [15], and double-sided LCC-compensated topology [16]. Similar to the inductive coupler, the capacitive coupler can be classified by its compensation topology and the corresponding characteristics are introduced as follows. The most common topology for capacitive coupler is the SN topology, in which only one series inductance is placed at either the transmitter or receiver side to compensate the coupling capacitance generated by metal plates [17], [18]. In this topology, a large coupling capacitance is required to achieve a reasonable

Manuscript received June 28, 2020; revised September 12, 2020; accepted October 23, 2020. Date of publication November 6, 2020; date of current version February 5, 2021. This work was supported in part by the National Natural Science Foundation of China under Grant 61471098, in part by the National Higher-Education Institution General Research and Development Project under Grants ZYGX2016J035 and ZYGX2018J037, and in part by the China Scholarship Council. Recommended for publication by Associate Editor M. Ponce-Silva. *(Corresponding authors: Yong-Ling Ban; Chunting Chris Mi.)*

Jia-Qi Zhu is with the School of Electronic Engineering, University of Electronic Science and Technology of China, Chengdu 611731, China, and also with the Department of Electrical and Computer Engineering, San Diego State University, San Diego, CA 92182 USA (e-mail: jia-qi.zhu@foxmail.com).

Yong-Ling Ban and Rui-Min Xu are with the School of Electronic Engineering, University of Electronic Science and Technology of China, Chengdu 611731, China (e-mail: byl@uestc.edu.cn; rmxu@uestc.edu.cn).

Chunting Chris Mi is with the Department of Electrical and Computer Engineering, San Diego State University, San Diego, CA 92182 USA (e-mail: mi@ieee.org).

Color versions of one or more of the figures in this article are available online at https://ieeexplore.ieee.org.

Digital Object Identifier 10.1109/TPEL.2020.3036459

switching frequency, leading to a small gap distance between the transmitter and receiver. A double-sided LCLC compensated topology was proposed in [9] and a 2.4-kW output power was transferred through a 150-mm air gap with 90.8% efficiency. To reduce the external compensated components, a double-sided LC compensated topology is investigated in [19]. A 150-W loosely coupled CPT system of 2.16% coupling coefficient was achieved with 180 mm air gap distance and the corresponding efficiency was higher than 70%. Different from [19], in this article, the compensated inductance is also used to transfer power, leading to an IPT-CPT-combined coupler which saves space and cost. Besides, the external parallel capacitances at the transmitter and the receiver side are different to adjust the power transfer ratio between IPT and CPT.

By reviewing IPT, CPT, and IPT-CPT combined systems, [20] depicted the advantages of IPT-CPT-combined system on power scaling capability, reduced compensation elements, higher link power transfer density, less pad compatibility issues, and improved misalignment tolerance, which indicates the necessity and imminent trend to combine IPT and CPT. Several techniques to achieve WPT through inductive and capacitive coupling have been investigated recently. As reported in [21] and [22], IPT-CPT-combined systems with LC-compensated topology were proposed for high power applications such as electric vehicles. In these two studies, the inductive coils for IPT and metallic plates for CPT are separately placed with a big air gap, indicating that the IPT coupler and CPT coupler are actually not integrated. The size of the combined coupler is the sum of the capacitive coupler and the inductive coupler. Besides, an inductive coil and two metal plates are required to be integrated at the receiving side. Thus, the systems in [21] and [22] are not suitable to be integrated into a compact smartphone. An inductive and capacitive integrated coupler with LCL compensation topology was studied in [23]. Both magnetic field and electric field were utilized in a single integrated coupler. However, the long-folded strip structure with 36 mm height was too large for smartphone applications and an external compensated inductance was required to adjust the power transfer ratio of IPT and CPT, which did not meet the compact requirement of a smartphone. In [24], an integrated IPT-CPT combined coupler was investigated for railway application. The metal plates were vertically arranged, and the coils were sandwiched between the metal plates. Although good misalignment ability is realized, this type of integrated coupler is not suitable for metal-cover smartphones because of the vertically arranged metal plates that cannot be used as metal cover, the 20-mm distance between the receiving coil and metal plate, as well as the eddy current loss without embedded ferrite. In [25] and [26], inductive and capacitive combined systems were reported for parallel transmission of power and data. In [25], the power is transferred by an electric field and in [26], the power is transferred by a tightly coupled transformer. Since the power and data were separately transferred by IPT and CPT, these systems are not dedicated to transfer power by magnetic field and electric field simultaneously. As indicated in [27], a distance-insensitive WPT system was proposed using mixed inductive and capacitive coupling. The magnetic coupling coefficient and electric coupling coefficient canceled each other so that the equivalent coupling coefficient in close range would be reduced, which suppressed frequency splitting phenomenon at small transmitting distance. The above-mentioned systems were all operated in free space condition. To achieve WPT through a metal barrier, a combined inductive and capacitive coupler was investigated in [28]. Two separate transmitting plates were employed to induce current flow in the metal barrier, thus generating a magnetic field on the secondary side. Here, the magnetic field was a horizontal-flux approach so that the pick-up coil inside the receiver was required to be perpendicular to the metal barrier, which was not suitable for smartphone applications. Besides, the size of the secondary compensating circuit was too big to be embedded in a mobile electronic device.

In [29], an NFC-CPT-combined coupler was proposed for metal-cover smartphone applications. Except for the structures of NFC antenna and metal plates, the proposed NFC-connected coupler in this article is completely different from the coupler in [29]. We need to emphasize here that the structures of the NFC antenna and metal plates (similar with [29]) are viewed as components that are already designed and existing in the proposed NFC-connected coupler. The main differences between [29] and the proposed coupler are indicated as follows. First, the coupler structures are different. An NFC antenna is connected to the metal plates (metal cover) in the proposed coupler, which makes the NFC antenna part of the WPT system. The power is transferred simultaneously by both the NFC antenna (IPT) and the metal cover (CPT). With regard to [29], the NFC antenna is glued onto the metal cover, but they are not connected, indicating that the NFC antenna is not part of the WPT system. The power is only transferred by the electric field between the metal plates (CPT). Besides, since the coupler in [29] only utilizes electric field to transfer power, the coil L at the transmitter side is not integrated with the coupler and it is only used for compensation. On the contrary, in this article, the Tx coil at the transmitter side is integrated with the proposed coupler, which is more compact than [29]. The Tx coil is used for both compensation and power transfer. Second, the circuit topologies are different. In [29], an SN topology is applied to the capacitive coupler. As for the proposed coupler in this study, two parallel capacitors are applied at the primary and secondary side for compensation and adjusting the power transfer ratio. Due to the different structure and circuit topology, the corresponding analyses method and design procedure are different.

In this article, an NFC-connected coupler using IPT-CPT combined wireless charging is proposed for metal-cover smartphone applications. To achieve WPT through metal cover and reduce eddy current loss, the metal cover itself is utilized as receiving plates for CPT. To constrain the voltage on the metal cover within a safety range, the compensated inductive coil for CPT is also used to transfer power, resulting in an IPT-CPT-combined coupler. Here, the NFC antenna first performs as the compensated inductance for CPT and also transfers power through the magnetic field, which has not been reported in any open literature based on our review. As the NFC-based mobile payment is becoming popular, NFC antenna has become a prerequisite component inside smartphones [30]. In the proposed coupler, the NFC antenna and metal cover that already exist in the smartphone are employed to be the receiving coil for IPT and

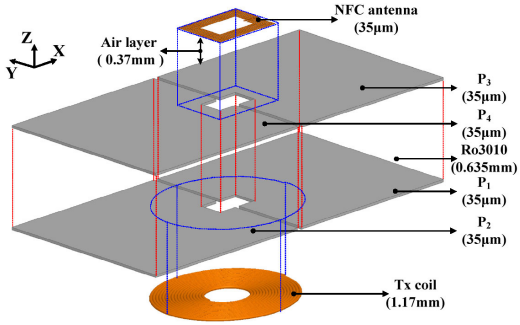

Fig. 1. Side view of the proposed NFC-connected coupler.

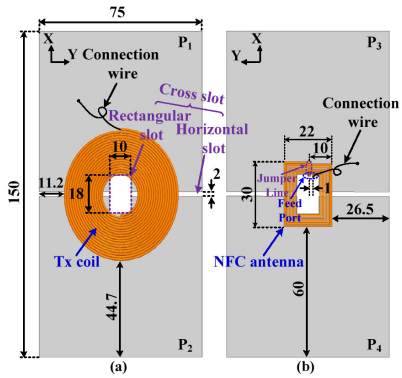

Fig. 2. (a) Plan view and (b) bottom view of the proposed NFC-connected coupler.

receiving plates for CPT, respectively. Thus, only one parallel compensated capacitor is needed to build the receiving coupler of the smartphone, which greatly saves cost for the WPT system. As is well known, the inductive coil for IPT and metal plates for CPT usually occupy most of the space in a WPT system. The use of the already existing planar NFC antenna that is fabricated by flexible printed circuit board (FPCB) and the metal cover also significantly saves space, which meets the compact requirement by smartphone applications.

II. Structure of the NFC-Connected Coupler

The side view of the proposed NFC-connected coupler using IPT-CPT-combined technology for smartphone is shown in Fig. 1, where connection wires are omitted for a better view. On the top and bottom of the stack are the transmitting coil (Tx coil) and receiving coil (NFC antenna). In the middle of the stack is the capacitive coupler, composed of two transmitting plates (P_1, P_2), two receiving plates (P_3, P_4), and the Ro3010 substrate ($\varepsilon_r = 10.2$) layer of 0.635 mm. It is noteworthy that the shape and dimension of the two receiving plates are the same as the transmitting plates. To utilize the Tx coil and NFC antenna as compensated inductor and realize IPT simultaneously, the Tx coil and NFC antenna are in conjunction with the metal plates P_1 and P_3, respectively. Here, the transmitting plates, Tx coil, and substrate layer construct the transmitter while the receiving plates (metal cover) and NFC antenna make up the receiver inside the smartphone.

The plan view of the proposed NFC-connected coupler is depicted in Fig. 2(a). The planer size of each metal plate is 74 mm $\times$ 75 mm, which corresponds to the size of an actual smartphone. Two transmitting plates P_1 and P_2 are separated by a cross-slot composed of a 2-mm width main horizontal slot and a rectangular slot (18 mm $\times$ 10 mm). In actual smartphones, the rectangular slot can represent the camera hole and flash hole. The horizontal slot is necessary for other antennas, such as WWAN/LTE/GPS. Above the transmitting plates, a Tx coil of 60.6 mm $\times$ 52.6 mm winds around the cross slot. In consideration of compactness and resonant frequency, AWG 44 Litz-wire of 300 strands is utilized to build the Tx coil and the winding width of which is 1.17 mm. It is noteworthy that the Tx coil is tightly winded with 17.5 turns and no air gap is introduced between each turn. The bottom view of the proposed NFC-connected coupler is shown in Fig. 2(b). The dimensions of the receiving plates (metal cover) are identical with the transmitting plates. The NFC antenna of 18 mm $\times$ 10 mm locates at the center of the metal cover. The line width and line gap of the NFC antenna are 0.8 and 0.4 mm, respectively. Here, the feed port locates at the top of the NFC antenna, where metal plate P_3 is linked to one of its feed lines through the connecting wire.

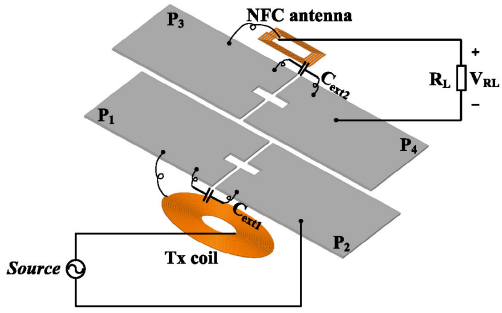

Fig. 3. Schematic circuit model of the proposed NFC-connected system.

III. Circuit Analysis

A. Circuit Model of the Proposed NFC-Connected System

The schematic circuit model of the proposed NFC-connected system is shown in Fig. 3, in which the connection and winding polarity can be viewed clearly. The 2.5-MHz sinusoidal source wave is generated by a power amplifier named AG 1016. To realize WPT through metal cover, the metal cover itself is utilized to be the receiving plates for CPT. In order to compensate the capacitive coupler and transfer inductive power, the Tx coil and NFC antenna are in conjunction with plate P_1 and P_3, respectively. Since the capacitive coupler is horizontally arranged, two external compensated capacitors C_{ext1} and C_{ext2} are employed to be parallel with the transmitting plates and receiving plates, respectively. According to (15), these two external capacitors can be tuned to adjust the power transfer ratio between IPT and CPT. It is worth noting that only one parallel capacitor is needed to construct the receiver for WPT inside the smartphone, which significantly reduces cost and saves valuable internal space for a smartphone.

Since the coupling capacitance can be generated by each two plates, six capacitances (C_{12}, C_{13}, C_{14}, C_{23}, C_{24}, and C_{34}) are generated among the four metal plates (P_1, P_2, P_3, and P_4). The equivalent circuit model of the four metal plates is

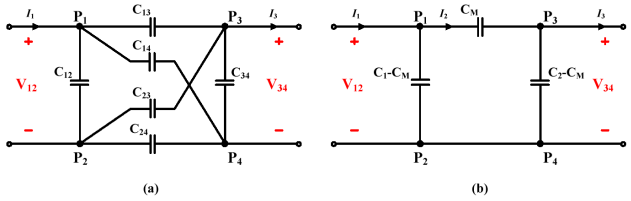

Fig. 4. (a) Six capacitance model of the four metal plates (P_1, P_2, P_3, and P_4). (b) Simplified π model of the four metal plates.

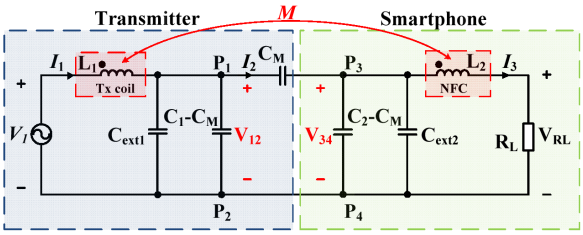

Fig. 5. Equivalent circuit model of the proposed NFC-connected system.

shown in Fig. 4(a). Based on [10], the six capacitance model can be simplified as π model, which is constructed by coupling capacitance C_M and self-capacitance C_1 and C_2, as depicted in Fig. 4(b). The relationship between the simplified π model and the six capacitances generated among the four metal plates is denoted as

$$\begin{cases} C_1 = C_{12} + \frac{(C_{13}+C_{14})\cdot(C_{23}+C_{24})}{C_{13}+C_{14}+C_{23}+C_{24}} \\ C_2 = C_{34} + \frac{(C_{13}+C_{23})\cdot(C_{14}+C_{24})}{C_{13}+C_{14}+C_{23}+C_{24}} \\ C_M = \frac{C_{24}C_{13}-C_{14}C_{23}}{C_{13}+C_{14}+C_{23}+C_{24}}. \end{cases} \tag{1}$$

As the four metal plates are represented by its simplified π model, the equivalent circuit model of the proposed system is depicted in Fig. 5. Since the Tx coil and NFC antenna are in conjunction with metal plates P_1 and P_3, L_1 represents the inductance of Tx coil and metal plate P_1, and L_2 represents the inductance of NFC antenna and metal plate P_3. Here, the polarity of the Tx coil and NFC antenna is significant that the inductive power and capacitive power are superposed at the output. Otherwise, the inductive power and capacitive power will weaken each other if the polarities of the two coils are reversed.

B. Working Principle of the Circuit

Before analyzing the circuit of the proposed NFC-connected system, capacitance $C_{\text{in}1}$ and $C_{\text{in}2}$ are defined as follows for simplification:

$$\begin{cases} C_{\text{in}1} = C_1 - C_M + C_{\text{ext}1} \\ C_{\text{in}2} = C_2 - C_M + C_{\text{ext}2}. \end{cases} \tag{2}$$

To study the working principle of the proposed IPT-CPT system, Kirchhoff's voltage law (KVL) is applied and the corresponding equation is expressed as

$$\begin{cases} (j\omega L_1 + \frac{1}{j\omega C_{\text{in}1}})I_1 - \frac{1}{j\omega C_{\text{in}1}}I_2 + j\omega M I_3 = V_1 \\ -\frac{1}{j\omega C_{\text{in}1}}I_1 + (\frac{1}{j\omega C_{\text{in}1}} + \frac{1}{j\omega C_M} + \frac{1}{j\omega C_{\text{in}2}})I_2 - \frac{1}{j\omega C_{\text{in}2}}I_3 = 0 \\ j\omega M I_1 - \frac{1}{j\omega C_{\text{in}2}}I_2 + (\frac{1}{j\omega C_{\text{in}2}} + j\omega L_2 + R_L)I_3 = 0. \end{cases} \tag{3}$$

By defining $R_{C\text{in}1}$, $R_{C\text{in}2}$, R_{CM}, R_{L1}, R_{L2} and R_M as the impedance of $C_{\text{in}1}$, $C_{\text{in}2}$, C_M, L_1, L_2, and mutual inductance M, the input current I_1 and output current I_3 are derived as (4), shown at the bottom of this page.

To achieve load-independent charging, $R_{C\text{in}1}(R_{C\text{in}2} + R_{CM}) + (R_{C\text{in}1} + R_{C\text{in}2} + R_{CM})R_{L1}$ needs to be zero and inductance L_1 is thus derived as

$$L_1 = \frac{C_{in2} + C_M}{\omega^2(C_{in2}C_M + C_{in1}C_M + C_{in1}C_{in2})}. \tag{5}$$

To realize zero phase angle (ZPA) at the input, $R_{C\text{in}2}(R_{C\text{in}1} + R_{CM}) + (R_{C\text{in}1} + R_{C\text{in}2} + R_{CM})R_{L2}$ should be zero and inductance L_2 is obtained as

$$L_2 = \frac{C_{in1} + C_M}{\omega^2(C_{in2}C_M + C_{in1}C_M + C_{in1}C_{in2})}. \tag{6}$$

With (5) and (6), (4) can be simplified as

$$\begin{cases} I_1 = V_1 \dfrac{(R_{C\text{in}1} + R_{C\text{in}2} + R_{CM})R_L}{R_{C\text{in}1}R_{C\text{in}2}(R_{CM}+2R_M) - (R_{C\text{in}1}+R_{C\text{in}2}+R_{CM})R_M^2 + R_{C\text{in}2}R_{L1}(R_{CM} + R_{C\text{in}1})} \\ \quad = V_1 R_L \left[\dfrac{(C_{\text{in}2}C_M + C_{\text{in}1}C_M + C_{\text{in}1}C_{\text{in}2})\omega}{C_M + (C_{\text{in}2}C_M + C_{\text{in}1}C_M + C_{\text{in}1}C_{\text{in}2})\omega^2 M}\right]^2 \\ I_2 = \dfrac{R_{C\text{in}1}(R_{C\text{in}2} + R_L + R_{L1}) - R_{C\text{in}2}R_M}{R_{C\text{in}1}R_{C\text{in}2}(R_{CM}+2R_M) - (R_{C\text{in}1}+R_{C\text{in}2}+R_{CM})R_M^2 + R_{C\text{in}2}R_{L1}(R_{CM} + R_{C\text{in}1})} \\ \quad = V_1 \dfrac{\omega^2 C_{\text{in}2}C_M(C_{\text{in}2}C_M + C_{\text{in}1}C_M + C_{\text{in}1}C_{\text{in}2})R_L - j\omega C_{\text{in}1}C_M[C_M + \omega^2 M(C_{\text{in}2}C_M + C_{\text{in}1}C_M + C_{\text{in}1}C_{\text{in}2})]}{[C_M + (C_{\text{in}2}C_M + C_{\text{in}1}C_M + C_{\text{in}1}C_{\text{in}2})\omega^2 M]^2} \\ I_3 = V_1 \dfrac{R_{C\text{in}1}R_{C\text{in}2} - R_M(R_{C\text{in}1}+R_{C\text{in}2}+R_{CM})}{R_{C\text{in}1}R_{C\text{in}2}(R_{CM}+2R_M) - (R_{C\text{in}1}+R_{C\text{in}2}+R_{CM})R_M^2 + R_{C\text{in}2}R_{L1}(R_{CM} + R_{C\text{in}1})} \\ \quad = V_1 \dfrac{-j\omega(C_{\text{in}2}C_M + C_{\text{in}1}C_M + C_{\text{in}1}C_{\text{in}2})}{C_M + (C_{\text{in}2}C_M + C_{\text{in}1}C_M + C_{\text{in}1}C_{\text{in}2})\omega^2 M}. \end{cases} \tag{7}$$

$$\begin{cases} I_1 = V_1 \dfrac{R_{C\text{in}2}(R_{C\text{in}1} + R_{CM}) + (R_{C\text{in}1} + R_{C\text{in}2} + R_{CM})(R_{L2} + R_L)}{R_{C\text{in}1}R_{C\text{in}2}(R_{CM} + R_{L1} + R_{L2} + 2R_M) - (R_{C\text{in}1} + R_{C\text{in}2} + R_{CM})(R_M^2 + R_{L1}R_{L2}) + R_{CM}(R_{C\text{in}1}R_{L2} + R_{C\text{in}2}R_{L1}) + [R_{C\text{in}1}(R_{C\text{in}2} + R_{CM}) + (R_{C\text{in}1} + R_{C\text{in}2} + R_{CM})R_{L1}]R_L} \\ I_3 = V_1 \dfrac{R_{C\text{in}1}(R_{C\text{in}2} - R_M) - R_M(R_{C\text{in}2} + R_{CM})}{R_{C\text{in}1}R_{C\text{in}2}(R_{CM} + R_{L1} + R_{L2} + 2R_M) - (R_{C\text{in}1} + R_{C\text{in}2} + R_{CM})(R_M^2 + R_{L1}R_{L2}) + R_{CM}(R_{C\text{in}1}R_{L2} + R_{C\text{in}2}R_{L1}) + [R_{C\text{in}1}(R_{C\text{in}2} + R_{CM}) + (R_{C\text{in}1} + R_{C\text{in}2} + R_{CM})R_{L1}]R_L} \end{cases} \tag{4}$$

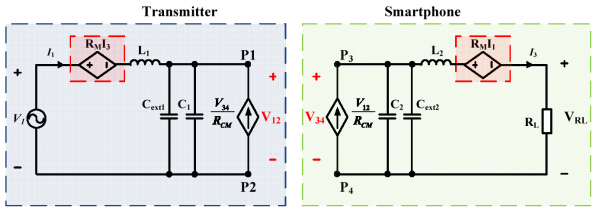

Fig. 6. Equivalent behavior source model of the proposed NFC-connected system.

From (7), the coil-to-coil efficiency η of the proposed system can be calculated as

$$\eta = \frac{I_3^2 R_L}{I_1^2 R_1 + I_3^2 R_2 + I_3^2 R_L}, \tag{8}$$

where R_1 and R_2 are the resistance of Tx coil and NFC antenna, respectively.

Based on (7), the gain G of Fig. 5 can be derived as

$$G = \left|\frac{V_{RL}}{V_1}\right| = \left|\frac{I_3 R_L}{V_1}\right| = \frac{\omega(C_{in2}C_M + C_{in1}C_M + C_{in1}C_{in2})R_L}{C_M + (C_{in2}C_M + C_{in1}C_M + C_{in1}C_{in2})\omega^2 M}. \tag{9}$$

The voltage V_{12} across P_1 and P_2 and the voltage V_{34} across P_3 and P_4 can be deducted as

$$\begin{cases} V_{12} = R_{Cin1}(I_1 - I_2) \\ \quad = R_{Cin1}V_1 \\ \quad \dfrac{(R_{Cin2} + R_{CM})R_L - (R_{Cin1}R_{Cin2} + R_{Cin1}R_{L1} - R_{Cin2}R_M)}{R_{Cin1}R_{Cin2}(R_{CM}+2R_M) - (R_{Cin1}+R_{Cin2}+R_{CM})R_M^2} \\ \quad + R_{Cin2}R_{L1}(R_{CM} + R_{Cin1}) \\ V_{34} = R_{Cin2}(I_2 - I_3) \\ \quad = R_{Cin2}V_1 \\ \quad \dfrac{R_{Cin1}R_L + R_{Cin1}R_{L1} + R_M(R_{Cin1} + R_{CM})}{R_{Cin1}R_{Cin2}(R_{CM} + 2R_M) - (R_{Cin1}+R_{Cin2}+R_{CM})R_M^2} \\ \quad + R_{Cin2}R_{L1}(R_{CM} + R_{Cin1}). \end{cases} \tag{10}$$

In order to obtain the power P_{IPT} transferred by the magnetic field and the power P_{CPT} transferred by the capacitive field, the behavior source model of the system is depicted in Fig. 6. Compared with the circuit model in Fig. 5, the magnetic coupling between the Tx coil and NFC antenna is represented by current-controlled voltage sources. The coupled voltage in each coil depends on the mutual inductance and the current flowing in the other coil. Besides, the electric coupling among the four plates is represented by voltage-controlled current sources, whose value depends on the voltage at the other side. Here, the apparent power S_{CPT} transferred by capacitive field can be calculated as

$$S_{\mathrm{CPT}} = V_{12}\left(-\frac{1}{R_{CM}}V_{34}\right)^*. \tag{11}$$

The symbol "$*$" in (11) represents the complex conjugate. From (11), the real power P_{CPT} is derived to be (12), shown at the bottom of this page.

The apparent power S_{IPT} transferred by magnetic field is expressed as

$$S_{\mathrm{IPT}} = -R_M I_1 I_3^*. \tag{13}$$

According to (13), the real power P_{IPT} is calculated as (14), shown at the bottom of this page.

In the proposed system, inductive power and capacitive power are transferred simultaneously, thus, the power transfer ratio is significant to be studied. Based on (12) and (14), the power transfer ratio R between IPT and CPT is derived as

$$R = \frac{P_{\mathrm{IPT}}}{P_{\mathrm{CPT}}} = \frac{\sqrt{(C_{in1} + C_M)(C_{in2} + C_M)}}{C_M}k. \tag{15}$$

Since the metal cover is used to transfer power and it will probably be touched by people during the charging process, the voltage V_{34} across the metal cover should be constrained within a safety range. According to [11] and [12], the voltage on the metal cover should be smaller than 8.35 V at HF.

Assuming that the output power is fixed as P, the required input voltage V_1 is deducted as follows based on (5)–(7):

$$V_1 = \sqrt{\frac{P}{R_L}}\frac{C_M + k\sqrt{(C_{in1} + C_M)(C_{in2} + C_M)}}{\omega(C_{in2}C_M + C_{in1}C_M + C_{in1}C_{in2})}. \tag{16}$$

By substituting (16) into (10), the rms value of V_{34} can be calculated as (17), shown at the bottom of the next page.

From (17), the optimum load resistance to realize the smallest voltage across the metal cover is derived as

$$R_L = \frac{[C_M + k\sqrt{(C_{in2} + C_M)(C_{in1} + C_M)}](C_M + C_{in1})}{\omega C_M(C_{in2}C_M + C_{in1}C_M + C_{in1}C_{in2})}. \tag{18}$$

$$P_{\mathrm{CPT}} = V_1^2 \frac{R_{Cin1}R_{Cin2}R_L}{R_{CM}} \frac{(R_{Cin1}R_{Cin2} + R_{Cin1}R_{L1} - R_{Cin2}R_M)R_{Cin1} + (R_{Cin2} + R_{CM})(R_{Cin1}R_{L1} + R_M(R_{Cin1} + R_{CM}))}{(R_{Cin1}R_{Cin2}(R_{CM} + 2R_M) - (R_{Cin1} + R_{Cin2} + R_{CM})R_M^2 + R_{Cin2}R_{L1}(R_{CM} + R_{Cin1}))^2} \tag{12}$$

$$P_{\mathrm{IPT}} = V_1^2 \frac{(R_{Cin1} + R_{Cin2} + R_{CM})[R_{Cin1}R_{Cin2} - R_M(R_{Cin1} + R_{Cin2} + R_{CM})]R_M R_L}{(R_{Cin1}R_{Cin2}(R_{CM} + 2R_M) - (R_{Cin1} + R_{Cin2} + R_{CM})R_M^2 + R_{Cin2}R_{L1}(R_{CM} + R_{Cin1}))^2} \tag{14}$$

TABLE I
SIMULATED PARAMETERS OF THE PROPOSED NFC-CONNECTED COUPLER

Parameter	Value	Parameter	Value
C_M	394.8 pF	C_1	396.8 pF
L_1	6 μH	L_2	0.57 μH
k	0.63		

TABLE II
SIMULATED PARAMETERS OF THE NFC-CONNECTED COUPLER WITH DIFFERENT DIELECTRIC MATERIALS

Parameters	Dielectric material				
	Ro3010	TMM 10	Ro3006	Glass	FR4
ε_r	10.2	9.2	6.15	5.5	4.4
C_M [pF]	394.8	356.9	237.6	212.6	174.3
C_1- C_M [pF]	2	2.2	1.2	1.1	2.3

TABLE III
MEASURED SPECIFICATIONS OF THE PROPOSED NFC-CONNECTED COUPLER

Parameter	Value	Parameter	Value
C_M	413.94 pF	C_1	425.86 pF
C_{ext1}	100 pF	C_{ext2}	5 nF
L_1	8.3 μH	L_2	0.77 μH
k	0.57	Q_1	30
Q_2	18.2	V_{12}	46 V
V_{34}	7.08 V	P_{IPT}	4.36 W
P_{CPT}	1.75 W	P	5.6 W
R_L	20 Ω	η	89.25 %
f_0	2.5 MHz		

IV. COUPLER DESIGN

ANSYS MAXWELL was utilized to simulate the parameters of the proposed NFC-connected coupler. The dimensions of the simulation model are the same as Figs. 1 and 2. The corresponding results are listed in Table I.

Compared with the measured parameters of the proposed coupler in Table III of Section VI, the difference between the simulated and measured parameters for C_1, C_M, and k are acceptable. However, the simulated self-inductances of L_1 and L_2 are smaller than the measured values, and the corresponding difference between them are relatively big. That is possibly because of the experimental wires shown in Fig. 16 and the four metal plates (P_1, P_2, P_3, and P_4) between the coils. In the proposed NFC-connected coupler, the inductance of the Tx coil and the NFC antenna are relatively small. Here, the experimental wires are necessary to conduct the experiment, but it is hard to be accurately modeled in the simulation, which contributes to the difference between the simulated and measured values. With regard to the four metal plates, they will reduce the inductance of the Tx coil and the NFC antenna. In the simulation, the impact of the four metal plates is possibly larger than that in the actual experiment. Above all, the measured parameters listed in Table III of Section V were used in the following analyses.

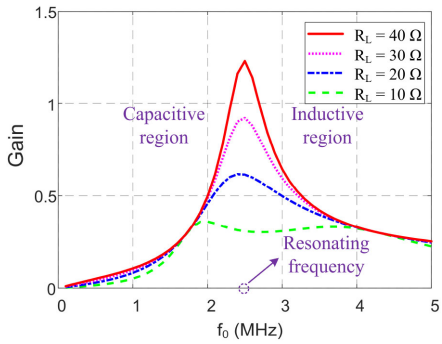

Fig. 7. Variation of gain for the proposed NFC-connected coupler regarding f_0 with different load resistances.

By substituting the passive parameters in Table III, the gain curve of the circuit in Fig. 5 is plotted as shown in Fig. 7. The resonating frequency is 2.5 MHz and f_0 represents the working frequency (switching frequency). With the increase of load resistance, the gain of the circuit will be enhanced. Before describing the design procedures of the proposed NFC-connected coupler, three basic requirements are necessary to be pointed out and they are listed as follows: 1) since the proposed coupler is applied to mobile consumer electronics, the external capacitor C_{ext1}, C_{ext2}, Tx coil L_1 inside the transmitter, and NFC coil L_2 inside the smartphone are required to be small to meet the compact requirement; 2) the coil-to-coil efficiency of the coupler should be as high as possible; and 3) the voltage V_{34} needs to be constrained within a safety range, which is 8.35 V (V_{safe}) at HF.

Next, the design procedures of the proposed NFC-connected coupler are discussed below. Four steps are needed to design and optimize the unknown parameters. The corresponding design flowchart is shown in Fig. 8.

1) Since the NFC antenna is embedded inside the smartphone, FPCB technology is used to fabricate the planar NFC antenna, leading to a very small total thickness of 0.4 mm. To achieve NFC through the metal cover, the shape and size of the metal plates are optimized and a cross slot is embedded on the metal cover, which mitigates the eddy current loss of the NFC antenna. For the detailed analyses, please see [29]. On the other hand, the separation of metal cover is also necessary to realize CPT because two detached receiving plates are required for CPT, indicating that the NFC antenna and CPT in the proposed coupler benefit each other. The detailed analyses and experiment of the NFC antenna are reported in [29]. Here, the NFC antenna is considered to be an already-designed and existing component inside the smartphone. Therefore, the inductance value L_2 of the NFC antenna is fixed, which was measured to be 0.77 μH.

$$|V_{34}| = \sqrt{P}\frac{\sqrt{\frac{\left[C_M+k\sqrt{(C_{in2}+C_M)(C_{in1}+C_M)}\right]^2(C_M+C_{in1})^2}{R_L}+\left(\omega C_M(C_{in2}C_M+C_{in1}C_M+C_{in1}C_{in2})\right)^2 R_L}}{\omega(C_{in2}C_M+C_{in1}C_M+C_{in1}C_{in2})[C_M+k\sqrt{(C_{in2}+C_M)(C_{in1}+C_M)}]} \tag{17}$$

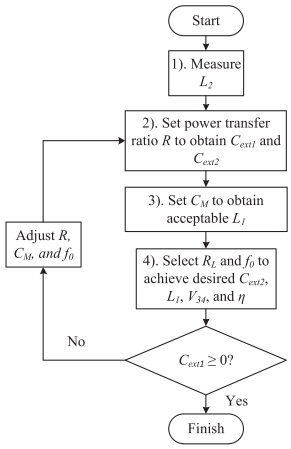

Fig. 8. Design flowchart of the proposed NFC-connected coupler.

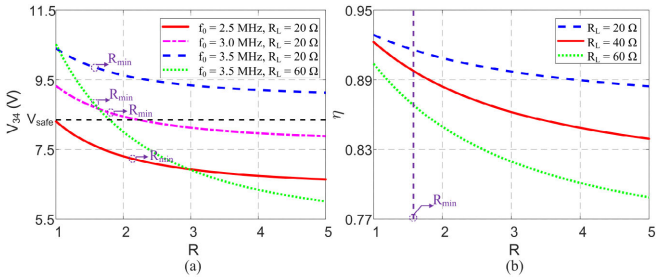

Fig. 9. (a) Variation of voltage V_{34} across the metal cover as a function of R with different resonating frequency and load resistance. (b) Coil-to-coil efficiency η as a function of R with different load resistances.

2) According to (6) and (15), the external capacitor C_{ext1} and C_{ext2} can be set to achieve the desired power transfer ratio. The external capacitor C_{ext1} is thus expressed as

$$C_{\text{ext1}} = \omega^2 L_2 \left[\left(\frac{R_{CM}}{k} \right)^2 - {C_M}^2 \right] - C_1. \tag{19}$$

The external capacitor C_{ext2} is expressed as

$$C_{\text{ext2}} = \frac{\left(\frac{R_{CM}}{k}\right)^2}{\omega^2 L_2 [\left(\frac{R_{CM}}{k}\right)^2 - {C_M}^2]} - C_2. \tag{20}$$

Here, the values of the external capacitors cannot be negative. With $C_{\text{ext1}} \geq 0$

$$R \geq k \sqrt{\frac{C_1}{\omega^2 L_2 {C_M}^2} + 1} = R_{\min}. \tag{21}$$

With $C_{\text{ext2}} \geq 0$ and (21)

$$\left(\frac{R}{k} \right)^2 (\omega^2 L_2 C_2 - 1) \leq \omega^2 L_2 C_2. \tag{22}$$

With L_2 and C_1 (C_1 equals C_2 due to symmetric property) of Table III, the operating frequency needs to be 8.8 MHz to make $\omega^2 L_2 C_2 - 1 = 0$. Since the operating frequency of a wireless charging system is normally smaller than 6.78 MHz, $\omega^2 L_2 C_2 - 1 \leq 0$. Equation (22) can be conducted as

$$\left(\frac{R}{k} \right)^2 \geq \frac{-\omega^2 L_2 C_2}{(1 - \omega^2 L_2 C_2)} \tag{23}$$

which is always true. With the parameters in Table III, R is required to be bigger or equal to 2.14 by (21). As indicated in Fig. 8, this requirement will be checked at the end of the procedure.

Since C_M has little impact on V_{34}, the voltage V_{34} as a function of power transfer ratio R is plotted with different resonating frequency and load resistance, as shown in Fig. 9(a). The output power for Fig. 9(a) is fixed as 5.6 W. According to the above discussion, the voltage V_{34} is required to be smaller than V_{safe}. Based on (21), the power transfer ratio R is required to be bigger than $R_{\min}$ and the load resistance R_L is not related to $R_{\min}$. With the increase of resonating frequency, $R_{\min}$ will be decreased. As shown in Fig. 9(a), the voltage V_{34} is decreased with the increase of R. That is because the voltage V_{34} across the metal cover is in proportion to the power transfer through CPT based on (11). In order to limit the voltage across the metal cover within a safety range and provide a wider tunable range for f_0 and R_L in the following steps, the power transfer ratio should be increased. If R is tuned to be small, the resonating frequency must be increased because $R_{\min}$ can be decreased with the increase of f_0. However, the increase of f_0 will lead to increased V_{34}. For example, if R is set below 2, the resonating frequency must be 3 or 3.5 MHz to decrease $R_{\min}$ in Fig. 9(a). In this case, the voltage V_{34} for the blue curve and magenta curve are above V_{safe}, which is not allowed. To fix this issue, the load resistance R_L can be increased, as shown in the green curve. However, the efficiency will decrease significantly with the increase of load resistance, as depicted in Fig. 9(b). Here, the resonating frequency for Fig. 9(b) is 3.5 MHz. For other resonating frequencies, similar results can be obtained in the required region ($R > R_{\min}$). Thus, R cannot be too small and needs to be increased. On the other hand, the current flowing in the Tx coil and the NFC antenna are in proportion to the power transferred by IPT based on (13). With the increase of current in the coils, the induced eddy current on the metal plates will increase, leading to increased loss [31]. If the coupler is integrated with a smartphone, more eddy current loss will be induced on the nearby metallic components inside the smartphone, leading to further decreased efficiency. Besides, with a fixed output power, the loss of the Tx coil will be increased due to the increase of input current I_1 (increased R), resulting in a lower efficiency of the proposed coupler, which is verified in Fig. 9(b). Therefore, the power transfer ratio should be reduced to increase efficiency. In consideration of both safety and eddy current loss, the power transfer ratio between IPT and CPT is selected to be 3.5/1.5.

3) Based on (2), (5), (19), and (20), L_1 is determined by C_1–C_M, C_M, and f_0 due to the symmetric property. Since the dimension of the proposed coupler is set in step 1), the proposed coupler is investigated with different dielectric materials, as listed in Table II. Compared with coupling capacitance C_M, the value change in C_1–C_M is much smaller regarding the dielectric layer. The inductance L_1 is thus determined by C_M and f_0.

With the variation of C_M, L_1, η, V_{34}, and C_{ext2} are calculated by (5), (8), (17), and (20). The output power for Fig. 10(c) is fixed

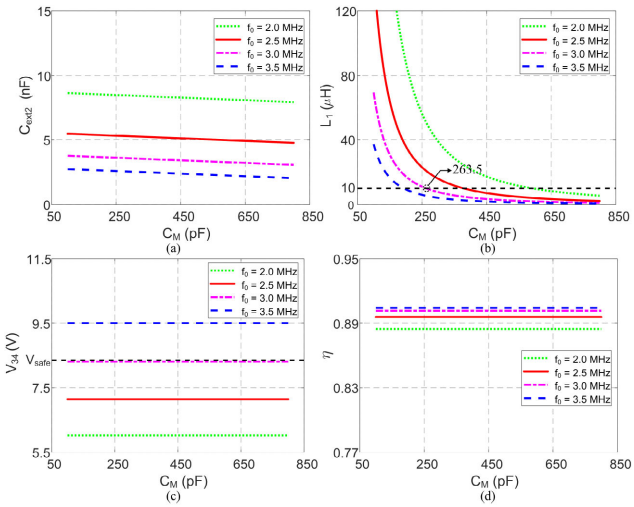

Fig. 10. Variation of (a) capacitance C_{ext2} inside the smartphone, (b) inductance L_1 of the Tx coil, (c) voltage V_{34} across the metal cover, and (d) coil-to-coil efficiency η as a function of coupling capacitance C_M with different resonating frequencies.

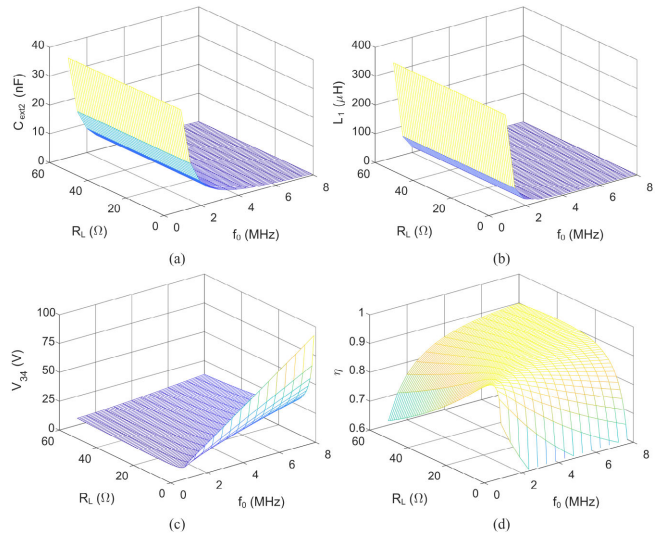

Fig. 11. Variation of (a) capacitance C_{ext2} inside the smartphone, (b) inductance L_1 of the Tx coil, (c) voltage V_{34} across the metal cover, and (d) coil-to-coil efficiency η regarding load resistance R_L and working frequency f_0.

as 5.6 W. The corresponding results with different resonating frequencies are shown in Fig. 10. Only L_1 changes significantly with C_M, whereas other three parameters nearly remain unchanged. According to Fig. 11, the operating frequency f_0 is relevant to C_{ext2}, L_1, V_{34}, and η. Therefore, C_M is first set by L_1 in this step.

As shown in Fig. 10(b), if the coupling capacitance C_M is small, the inductance L_1 will become large, making the Tx coil too large to be embedded in the transmitter. Thus, C_M needs to be increased to reduce the inductance of the Tx coil. The inductance of L_1 is required to be smaller than 10 μH in this design. It is noteworthy that this upper limit for L_1 can be increased if a ferrite sheet is integrated into the transmitter. As shown in Fig. 10(c), V_{34} will exceed or reach V_{safe} if the resonant frequency is 3 and 3.5 MHz, indicating that f_0 must be smaller than 3 MHz. As shown in Fig. 10(b), to limit L_1 within 10 μH, C_M must be bigger than 263.5 pF, indicating that a dielectric layer is necessary to be integrated in the transmitter. In this case, the available Ro3010 and TMM 10 from Table II can be selected as the dielectric material to achieve acceptable C_M. Because higher C_M leads to bigger tunable range for f_0, the available Ro3010 dielectric layer with 0.635 mm thickness is finally selected, leading to suitable measured C_M of 413.9 pF. It is noteworthy that other dielectric layers with different thicknesses can be applied as long as the resultant C_M meets the requirement in Fig. 10(b) and (c).

4) Based on (5), (19), and (20), with the selected C_M, C_1, C_2, and fixed L_2, the parameters of the coupler can be set with the load resistance R_L and resonating frequency f_0. To find the optimum value of load resistance R_L and resonating frequency f_0, the compensated external capacitor C_{ext2}, inductance L_1 of the Tx coil, voltage V_{34} across the metal cover and the coil-to-coil efficiency η are studied. With the variation of load resistance and resonating frequency, L_1, η, V_{34}, and C_{ext2} are calculated by (5), (8), (17), and (20). The corresponding results are depicted in Fig. 11(a)–(d), respectively. It is noteworthy that the equivalent resistance R_1 of the Tx coil and R_2 of the NFC antenna are taken into consideration to obtain Fig. 11(d). From Fig. 11(a) and (b), it can be seen that the external capacitance C_{ext2} and inductance L_1 are independent of R_L. With the increase of resonating frequency, C_{ext2} and L_1 will first decrease sharply and then decrease slowly. Besides, as shown in Fig. 11(c), the voltage across the metal cover will increase with the enhancement of resonating frequency, indicating that the resonating frequency cannot be too high. In consideration of both space and safety (voltage across the metal cover), the resonating frequency is finally selected as 2.5 MHz.

As shown in Fig. 11(d), the optimum coil-to-coil efficiency η appears at 13 Ω load resistance with 2.5 MHz working frequency. However, the corresponding voltage V_{34} across the metal cover will be 8.34 V, which almost exceeds the safety range. As indicated in Fig. 11(c), the lowest V_{34} comes with 40 Ω load resistance at 2.5 MHz working frequency but the corresponding coil-to-coil efficiency η is relatively low as 84.5%. Above all, a suitable value of 20 Ω is used for load resistance R_L, which lies between 13 and 40 Ω. The calculated corresponding voltage V_{34} and coil-to-coil efficiency η are 7.14 V and 89.6%, respectively.

According to (21) of step 2), the power transfer ratio needs to be bigger than $k\sqrt{\frac{C_1}{\omega^2 L_2 {C_M}^2}+1} \approx k\sqrt{\frac{1}{\omega^2 L_2 C_M}+1}$ in consideration of C_{ext1}. After selecting the operating frequency, the external capacitor C_{ext1} can be calculated by (19). According to step 3), C_M is required to be relatively big to decrease L_1. Based on step 4), f_0 cannot be too large in consideration of V_{34}. Thus, the value of $k\sqrt{\frac{1}{\omega^2 L_2 C_M}+1}$ is relatively small and the selected power transfer ratio will normally meet the requirement of (21). For example, the required minimum power transfer ratio calculated by (21) is 2.14, indicating that selected power transfer ratio of 3.5/1.5 meets the requirement. As indicated in Fig. 8, to

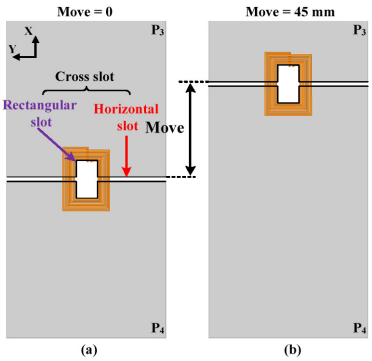

Fig. 12. Movement of the cross slot together with Tx coil and NFC antenna. (a) Move = 0. (b) Move = 45 mm.

make sure that the design is reasonable, the calculated C_{ext1} is still checked at the end. If the calculated C_{ext1} is negative, the designed parameters need to be adjusted.

V. Practical Consideration

A. Cross-Slot Location

For practical consideration, the rectangular slot may represent the camera hole or fingerprint, which normally locates at the top of the back cover in smartphones nowadays. Here, we need to state that the location of cross slot for the proposed coupler does not have to be placed at the middle of the metal plates. The location of the slot can be varied to fit in different smartphones. For example, the cross slot can be placed at the top half of the metal cover as in present-day smartphones, as shown in Fig. 12(b). For the fabricated coupler, the cross slot is placed at the middle of metal plates to achieve maximum coupling capacitance C_M and verify the circuit analysis in Section III.

For movement analyses, the cross slots in the four metal plates together with the NFC antenna and Tx coil are moved from the middle to the top, as shown in Fig. 12. With the movement, the passive parameters of the proposed coupler are simulated in ANSYS MAXWELL. The inductance L_1 of the Tx coil, the inductance L_2 of the NFC antenna and the coupling coefficient k remain unchanged, indicating that L_1, L_2, and k are not influenced by the movement. Here, C_{sum1} is defined as

$$C_{\mathrm{sum1}} = C_1 - C_M. \tag{24}$$

The capacitances C_M and C_{sum1} regarding movement of the cross slot are depicted in Fig. 13. It can be seen that only coupling capacitance C_M is reduced with the move of the cross slot. According to the analyses on C_M in Section IV, step 3), only L_1 of the Tx coil will increase significantly with the decrease of C_M whereas other parameters remain unchanged. The Tx coil is supposed to be integrated in the transmitter, which locates outside of the smartphone. Since the volume of transmitter is not strictly restricted compared with the smartphone, the enlarged Tx coil with increased inductance is actually able to be embedded in the transmitter, indicating that the cross slot does not really impact the proposed coupler.

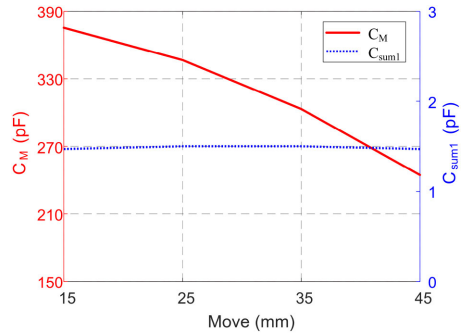

Fig. 13. Variation of capacitances C_M and C_{sum1} regarding movement.

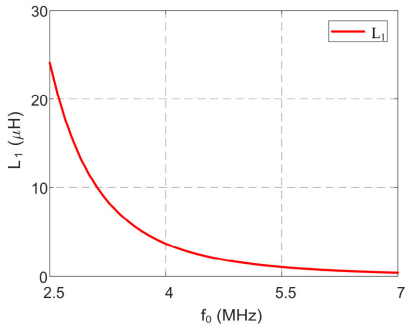

Fig. 14. Variation of inductance L_1 as a function of operating frequency when Move = 45 mm.

If both the transmitter and smartphone are required to be small and compact, the impact of cross-slot movement (increased L_1) can be fixed in three ways. It is noteworthy that the following three methods are applied to Fig. 12(b) with Move = 45 mm. The corresponding C_M and L_1 are 244.5 pF and 24 μH without optimization.

1) Reduce the Thickness H of the Dielectric Layer: Since the distance between the Tx coil and NFC antenna is very small for the proposed coupler, reducing the thickness of the dielectric layer from 0.635 to 0.381 mm will not influence the coupling coefficient k. Self-inductance L_1 and L_2 will not be affected with the variation of H. If the thickness of dielectric layer is reduced from 0.635 to 0.381 mm, C_M (Move = 45 mm) will be increased to 408.8 pF, which is similar to the original coupling capacitance. Therefore, the characteristic of the coupler with 45 mm movement can be made the same as the proposed coupler, indicating that the location of the cross slot can be varied for different smartphones.

2) Increase the Operating Frequency f_0 and Adjust R_L: Based on (5), (19), and (20), the compensated inductance L_1 is determined by f_0 and C_M if the power transfer ratio R is fixed. When the cross slot moves 45 mm, L_1 as a function of f_0 is depicted in Fig. 14. The operating frequency can be selected as 3.2 MHz to obtain acceptable L_1, whose value is 8.97 μH. According to (17), the voltage V_{34} across the metal cover will be increased to 8.79 V, which is beyond the safety range. To reduce V_{34} within the safety range, the load resistance R_L can be adjusted to 28 Ω. The corresponding V_{34} is 7.88 V and the

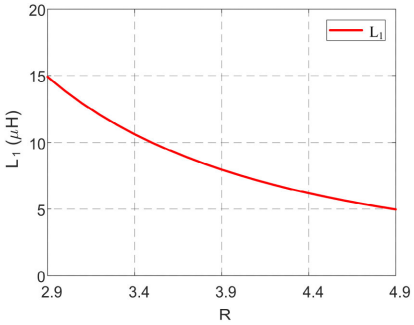

Fig. 15. Variation of inductance L_1 as a function of power transfer ratio when Move = 45 mm.

calculated efficiency is 89.18%, which is similar to the proposed coupler with the cross slot in the middle.

3) Increase the Power Transfer Ratio R Between IPT and CPT: If the power transfer ratio is increased, the external capacitor C_{ext1} will be increased based on (19), leading to the decrease of L_1. The relationship between R and L_1 is plotted in Fig. 15. If R is increased from 3.5/1.5 to 3.6, L_1 will be decreased to 9.4 μH. The corresponding V_{34} and η will be 6.43 V and 87.94%, which is acceptable and similar to the proposed coupler with the cross slot in the middle.

The three methods mentioned above can be used together to reduce L_1. For example, if R is increased to 3 and f_0 is increased to 2.9 MHz, L_1 will be 7.66 μH. The corresponding V_{34} and η will be 7.88 V and 89.2%, respectively. In conclusion, the cross slot does not have to be placed at the middle of the metal plates. The position of the cross slot can be varied to meet the requirements of different smartphones.

B. Misalignment Analyses

To investigate the transmission performance regarding misalignment, X- and Y-axis are defined in Fig. 1. Since the NFC antenna and metal plates P_3 and P_4 are supposed to be integrated inside the smartphone, they are moved along X- and Y-axis for misalignment analyses. The transmission performance (misalignment ability) is only investigated within 25 mm of the misalignment. That is because the output power becomes too small when misalignment exceeds 25 mm, which will make the analyses meaningless. The corresponding simulated parameters are shown in Figs. 16 and 17. With the simulated parameters at no misalignment case, the external capacitors C_{ext1} and C_{ext2} are calculated to be 300 pF and 6.89 nF by (19) and (20) and remain unchanged during the misalignment analyses. For the capacitive part of the coupler, the coupling capacitance C_M will decrease with the increase of X and Y misalignment. With the increase of X misalignment, C_{in1} and C_{in2} will increase but the variation of C_{in2} is much smaller than C_{in1}. That is because C_{in2} is mainly determined by the fixed C_{ext2} and the increase of $C_2 - C_M$ is much smaller than the value of C_{ext2}. With the increase of Y misalignment, both C_{in1} and C_{in2} will remain nearly unchanged. With regard to the inductive part of the coupler, the inductance L_1 and L_2 will decrease with the increase of X and Y misalignment. Here, the reductions of L_1 and

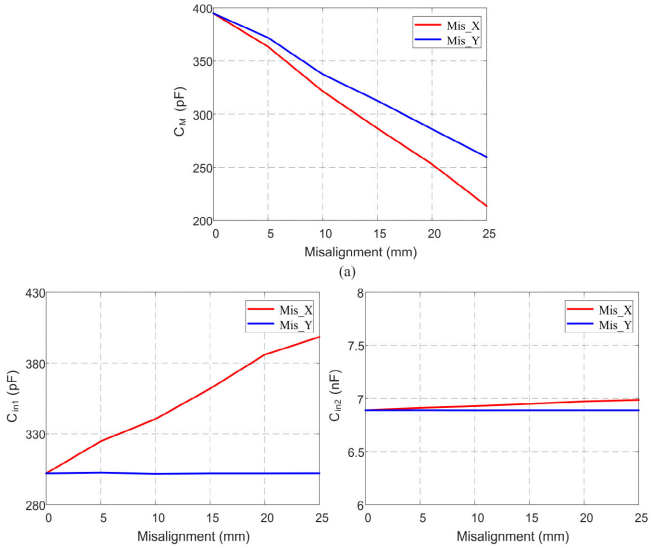

Fig. 16. Variation of (a) coupling capacitance C_M, (b) capacitance C_{in1}, and (c) capacitance C_{in2} of the NFC-connected coupler regarding X and Y misalignment.

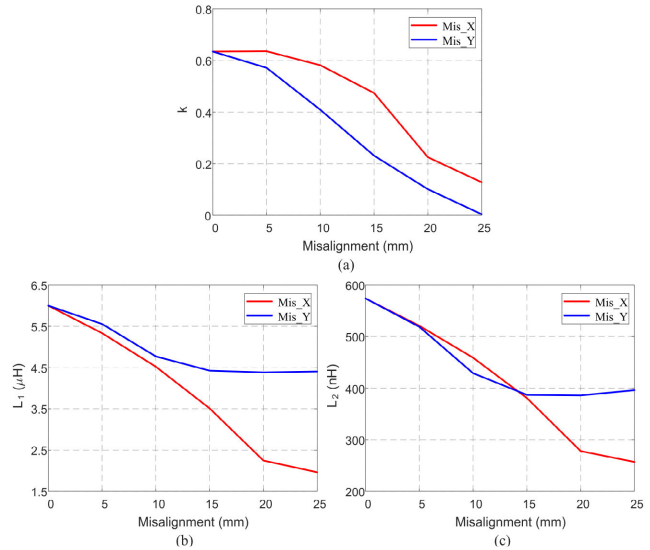

Fig. 17. Variation of (a) coupling coefficient k, (b) self-inductance L_1, and (c) self-inductance L_2 of the proposed NFC-connected coupler regarding X and Y misalignment.

L_2 come from the four metal plates and the width of the NFC antenna is only 22 mm. When Mis_Y = 20 mm, the NFC antenna moves away from the transmitting plates (P_1 and P_2), leading to a reduced impact from the transmitting metal plates to the NFC antenna. As a result, the inductance L_2 will increase with misalignment if Mis_Y > 20 mm. When Mis_Y = 45 mm, the impact from the transmitting plates on the NFC antenna becomes negligible. Thus, the inductance of L_2 will remain unchanged if Mis_Y exceeds 45 mm. With the increase of misalignment, the coupling coefficient k will decrease. Because the widths of the Tx coil and the NFC antenna are smaller than their lengths, the variation of k on Y misalignment is bigger than X misalignment.

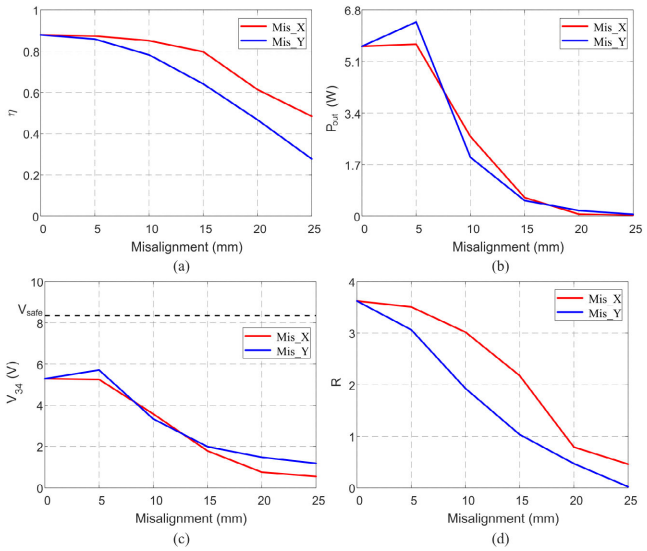

Fig. 18. Variation of (a) coil-to-coil efficiency η, (b) output power, (c) voltage V_{34}, and (d) power transfer ratio R of the proposed NFC-connected coupler regarding X and Y misalignment.

From (4), the output power P_{out} can be calculated as

$$P_{\text{out}} = I_3^2 R_L. \tag{25}$$

The circuit efficiency can be calculated by (8). With I_1 and I_3 of (4), the voltage V_{34} across the metal cover is conducted as

$$V_{34} = I_3 R_L + I_3 R_{L2} + R_M I_1. \tag{26}$$

The voltage V_{12} across the metal cover is expressed as

$$V_{12} = V_1 - R_M I_3 - R_{L1} I_1. \tag{27}$$

With (4), (26), and (27), the power transfer ratio R can be calculated by (11) and (13).

With V_1 of 12.5 V, R_L of 20 Ω, capacitances at different misalignment (see Fig. 16), inductances and coupling coefficients at different misalignment (see Fig. 17), the corresponding calculated efficiency η, output power P_{out}, voltage V_{34}, and power transfer ratio R are shown in Fig. 18(a)–(d), respectively. As shown in Fig. 18, the circuit efficiency, output power, voltage V_{34}, and power transfer ratio will decrease with the increase of misalignment. Because a voltage source V_1 is applied for analysis, the output power is increased a little when Mis_$Y = 5$ mm, leading to a slight increase of voltage V_{34}. Since the planar size of the NFC antenna is much smaller than the metal plates, with the same misalignment, the variation of inductive coupling between coils will be bigger than the capacitive coupling between the metal plates. Therefore, the power transfer ratio is decreased with the increase of misalignment. When Mis_$Y =$ 25 mm, R becomes nearly zero because the coupling coefficient k is nearly zero.

C. Implementation for NFC and the NFC-Connected System

Considering a real working scenario, the NFC and WPT system will not work at the same time. The reasons are explained as follows.

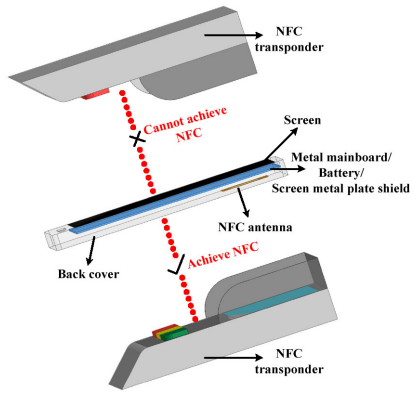

Fig. 19. Schematic diagram of the NFC working principle.

1) As indicated in [30], because of the severe limited operation range, the NFC indicates users' intent. When you point, where you point, or at whom you point, tells the machine about what it is supposed to do. The essential difference between the NFC antenna and far field antenna (such as Wi-Fi and LTE) is that people will only use NFC antenna when they intend to do something while the far field antenna is sending and receiving information all the time. So, if people would like to use NFC antenna, they must first grab the smartphone and then point the back of the smartphone to the NFC transponder, such as mobile payments, public transport, smart poster, and door access. With regard to present-day WPT system, the smartphone needs to be placed on a charging pad to realize wireless charging. Thus, if a smartphone is being charged on a charging pad and people need to use NFC function, they will need to first grab the smartphone from the charging pad and then point it to an NFC transponder. After that, the smartphone can be put back to the charging pad and continue to be charged.

2) As shown in Fig. 19, the NFC antenna is placed at the backside of the smartphone. Since the metallic components, such as metal mainboard and/or battery and/or screen metal shield, etc., are embedded above the NFC antenna, the NFC antenna can only communicate with the NFC transponder from the back side of the smartphone. With regard to WPT, the capacitive plates or inductive coil are integrated at the bottom of the smartphone and the wireless charging is realized through the back cover. When the smartphone is being charged wirelessly, the back cover of the smartphone is attached to the charging pad so that near field communication cannot be proceeded.

Above all, the NFC antenna and proposed NFC-connected coupler will not operate at the same time. As shown in Fig. 20, a simple switch with single pole double throw (SPDT) function can be used to switch from the NFC and WPT. The NFC device and the proposed coupler will not disturb each other. The 2.5-MHz current of the IPT-CPT combined system will not go through the NFC chip and the 13.56-MHz current of the NFC system will not go through the IPT-CPT combined system. Therefore, only the NFC antenna is required to stand both the 2.5-MHz current and the 13.56-MHz current. The 0.8-mm line width of the NFC antenna is enough to handle the current of the proposed NFC-connected coupler and the NFC system.

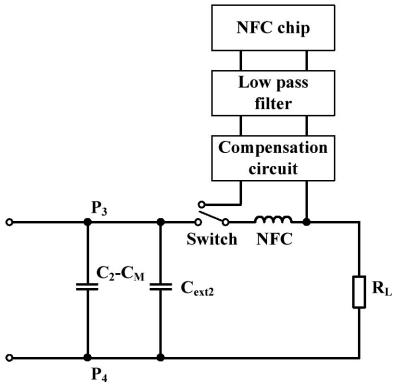

Fig. 20. Schematic diagram for possible implementation of NFC and WPT.

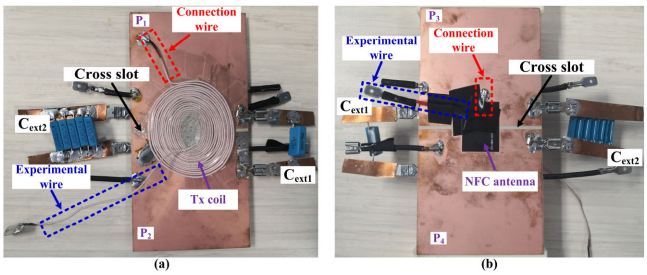

Fig. 21. (a) Top view and (b) bottom view of the fabricated prototype for the proposed NFC-connected coupler.

VI. Experiment and Discussion

A. Experiment on the Sole Proposed Coupler (Case A)

The prototype of the proposed NFC-CPT-connected coupler for metal-cover smartphone applications was fabricated and tested, as shown in Fig. 21. At the transmitter side, two metal plates (P_1 and P_2) of 35 μm thickness were mounted on the Ro3010 substrate layer of 0.635 mm thickness, as shown in Fig. 21(a). To compensate and adjust the power transfer ratio, compensation capacitance C_{ext1} of 100 pF was soldered in parallel with the metal plates. On top of the transmitter stack was the Tx coil, one feed line of which was connected to metal plate P_1. The Tx coil was fabricated by AWG 44 Litz-wire with 300 turns. Here, Litz wire was utilized because it was easy to fabricate and adjust, which is good for conducting the experiment. In practice, since the current flowing through the Tx coil is very small as 0.36 A, the Tx coil can be fabricated by printed circuit board (PCB) to further reduce the volume of the proposed coupler. With the designed inductance of L_1, the shape and size of Tx coil can also vary to fit with the other components inside the transmitter. At the receiver side, compensation capacitance C_{ext2} of 5 nF was soldered in parallel with metal plates P_3 and P_4 (metal cover), as depicted in Fig. 21(b). At the center of the metal cover, the NFC antenna was wound around the cross slot and in conjunction with metal plate P_3 through the connection wire. To save space for smartphones, the NFC antenna was fabricated by FPCB with polyimide (PI, $\varepsilon_r = 3$) base material. In real industrial applications, the cross slot represents the possible camera hole, flash hole, and main horizontal slot.

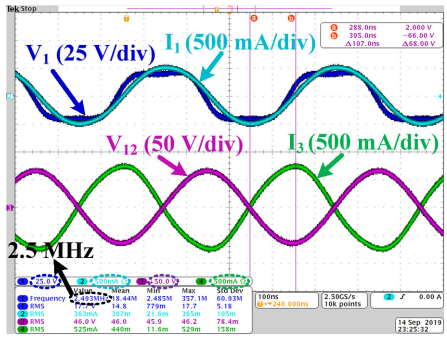

Fig. 22. Experimental waveforms of the proposed NFC-connected coupler.

It is noteworthy that convenient and available film capacitors were utilized here for research and verification. In practical applications, film capacitors should be replaced by small ceramic capacitors to save space inside the smartphone. Due to the relatively low voltage rating requirement for external capacitors of the proposed coupler, it is easy to select a suitable ceramic capacitor model with small packaging. For example, the C0603C510F2GACTU (51 pF) with 0603 packaging from KEMET can be used to fabricate C_{ext1} and the C0603C102F5GACTU (1 nF) with 0603 packaging from KEMET can be utilized to build C_{ext2}.

To conduct the experiment for the proposed NFC-connected coupler, an AG 1016 power amplifier from T&C Power was utilized to provide the 2.5-MHz ac waveform. After integrating the proposed coupler with the power amplifier and load resistance of 20 Ω, 5.6 W output power was achieved with 89.3% coil-to-coil efficiency. The corresponding experimental waveforms and test results are shown in Fig. 22 and Table III, respectively. It is noteworthy that the scales of the waveforms are denoted with labels and marked by dotted circles. Here, the input voltage V_1 was nearly in phase with the input current I_1 and the phase difference between the input current and output current was 96.3° (107 ns at 2.5 MHz). With 5.6 W output power, the voltage V_{34} across the metal cover was measured to be 7.08 V, which met the safety requirement (8.35 V). It is noteworthy that the measured P_{IPT} was calculated by $\omega M|I_1 I_3| \sin\theta_I$ and the measured P_{CPT} was calculated by $\omega C_M|V_{12}V_{34}| \sin\theta_V$, where θ_I indicates the phase difference between I_1 and I_3 and θ_V represents the phase difference between V_{12} and V_{34}. In this case, 4.36 W power was transferred by magnetic field and 1.75 W power was transferred by electric field.

With a fixed output power, the load resistance is varied to verify the circuit characteristic of the proposed coupler. In Fig. 23, the experimental input voltage V_1 and voltage V_{34} across the metal cover correspond well with the calculated values. However, noticeable difference exists between the calculated values and experimental values for input current I_1 and voltage V_{12}. Since the inductance L_2 of the NFC antenna is very small (0.77 μH), measurement of L_2 may be inaccurate. If the inductance of the NFC antenna decreases to 0.63 μH, the revised-calculated results are plotted in Fig. 23 as green curves for comparison. As shown in Fig. 23, nearly no difference exists between the revised-calculated V_{12} and the measured V_{12}. With

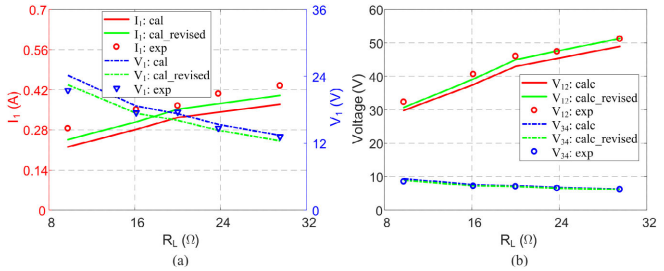

Fig. 23. Experimental, calculated, and revised-calculated (a) input current I_1 and input voltage V_1, and (b) voltage V_{12} across the transmitting plates and voltage V_{34} across the metal cover at different load resistance R_L.

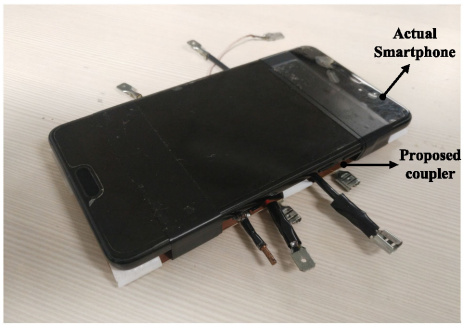

Fig. 24. Fabricated prototype of the proposed coupler with integrated smartphone.

regard to the input current I_1, the difference is reduced but 9% average difference still exists between the revised-calculated values and measured values. That is possibly because of the measurement error of the oscilloscope and the current probe, which is generated by the small value of I_1 (within 0.5 A).

B. Experiment on the Proposed Coupler With the Integrated Smartphone (Case B)

In practical consideration, the proposed coupler was integrated with an actual smartphone for experiment. Huawei Mate 10 was selected as the actual smartphone because its planar size is 150.5 mm × 77.8 mm, which is nearly the same as the proposed coupler. Since the back cover of Huawei Mate 10 is nonmetallic, the metal plates P_3 and P_4 of the proposed coupler become the metal cover for the smartphone. As shown in Fig. 24, the smartphone was integrated with the proposed coupler by insulation tape. The distance between the coupler and the smartphone was 2 mm, which was caused by the necessary experimental wire shown in Fig. 21(b). For better understanding, Case A represents the proposed coupler without the integrated smartphone and ferrite, Case B represents the proposed coupler with the integrated smartphone, and Case C represents the proposed coupler with the integrated smartphone and ferrite sheet.

Since all the components, including mainboard, battery, camera etc., of the smartphone were included in the experimental prototype, it is not applicable to analyze the influence from every component inside the smartphone on the metal plates for CPT and inductive coils for IPT. The smartphone was viewed as a whole and set as an external condition for the proposed coupler. With the smartphone, the passive parameters of the proposed coupler were measured, as listed in Table IV. Compared with the parameters in Table III (Case A), the inductances of Tx coil and NFC antenna are significantly decreased. That is due to the reflection impedance of the metallic components (e.g., battery and mainboard) inside the smartphone [32]. With regard to capacitances C_1, C_2, and C_M with the smartphone (Case B), they change little as compared with the original prototype (Case A). Based on (2), (5), and (6), external capacitor C_{ext1} of 300 pF and C_{ext2} of 7.8 nF are used for compensation. With the variation of load resistance, the experimental coil-to-coil efficiency η and the measured voltage V_{34} across the metal cover are depicted as red curves in Fig. 25(a) and (b), respectively. Here, the measured efficiency with the smartphone for Case B is much smaller than the efficiency for Case A. For example, the measured efficiency at 20 Ω is 74.28% for Case B and 89.25% for Case A. That is mainly because of the induced eddy current loss on the metallic components inside the smartphone. With regard to V_{34} at different load resistances, it is smaller than the values of the original coupler [Case A, Fig. 23(b)]. For example, the voltage V_{34} at 20 Ω load resistance is 5.32 V for Case B and 7.08 V for Case A. That is because the external capacitances C_{ext1} and C_{ext2} are changed for the coupler with smartphone (Case B), leading to bigger power transfer ratio R of 3.39 according to (15). With the same output power, the power transferred by CPT is smaller with the integrated smartphone (Case B), resulting in a smaller V_{34}. Here, the voltages V_{34} at different load resistances are all within the safety range (8.35 V). The experimental waveforms with 20 Ω load resistance for Case B are shown in Fig. 26. Compared with the waveforms in

TABLE IV
EXPERIMENTAL PARAMETERS OF THE PROPOSED COUPLER WITH INTEGRATED SMARTPHONE

Parameter	Value	Parameter	Value
C_M	419.3 pF	C_1	453.8 pF
C_{ext1}	300 pF	C_{ext2}	7.8 nF
L_1	5.78 μH	L_2	0.508 μH
k	0.57	R_L	20 Ω
η	74.28 %	V_{34}	5.32 V
R	3.55		

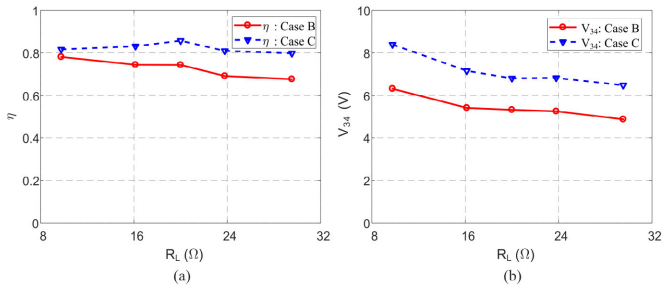

Fig. 25. (a) Measured efficiency η and (b) voltage V_{34} across the metal cover for Case B and Case C.

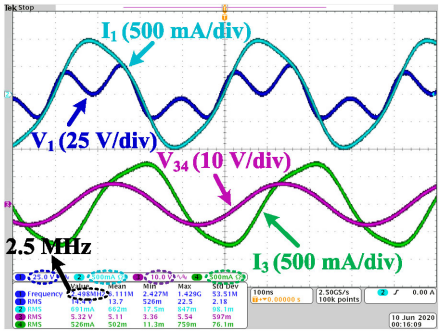

Fig. 26. Experimental waveforms of the proposed coupler with integrated smartphone (Case B).

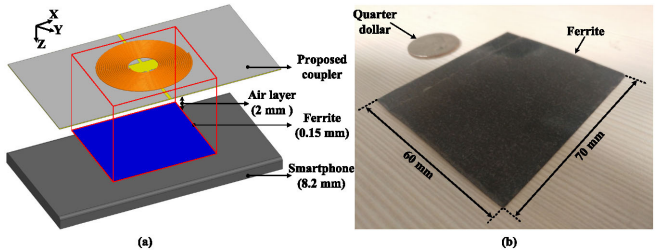

Fig. 27. (a) Schematic diagram of the proposed coupler with integrated smartphone and ferrite (Case C). (b) Embedded flexible ferrite composite sheet.

TABLE V
EXPERIMENTAL PARAMETERS OF THE PROPOSED COUPLER WITH INTEGRATED SMARTPHONE AND FERRITE

Parameter	Value	Parameter	Value
C_M	419.3 pF	C_1	453.8 pF
C_{ext1}	100 pF	C_{ext2}	5.4 nF
L_1	7.776 μH	L_2	0.73 μH
k	0.687	R_L	20 Ω
η	85.7 %	V_{34}	6.8 V
R	3.02		

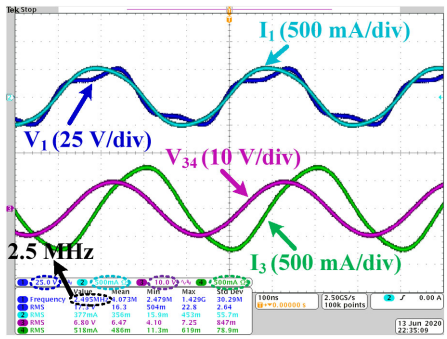

Fig. 28. Experimental waveforms of the proposed coupler with integrated smartphone and ferrite (Case C).

Fig. 22 (Case A), the waveforms with the smartphone (Case B) were distorted to a certain extent.

C. Experiment on the Proposed Coupler With the Integrated Smartphone and Ferrite Sheet (Case C)

From the above analyses, the passive parameters regarding CPT (C_1, C_2, and C_M) change little with the integrated smartphone, whereas the passive parameters regarding IPT (L_1 and L_2) change significantly. Besides, according to [9], the efficiency of an inductive coupler will drop significantly due to the induced eddy current on nearby metal object, whereas the electric field of capacitive coupler does not generate significant loss. Therefore, the impact of the integrated smartphone mainly comes from IPT rather than CPT. To mitigate the impact of the smartphone and enhance efficiency, a flexible ferrite composite sheet of 70 mm × 60 mm × 0.31 mm was embedded between the coupler and the smartphone, as indicated in Fig. 27(a). The utilized ferrite sheet was shown in Fig. 27(b) and the quarter-dollar was used as a reference. The material of the ferrite sheet is AFS-150-R10-A-20-30 from AMO with a relative permeability of 140 at 2.5 MHz.

The measured parameters of the proposed coupler with the integrated smartphone and ferrite (Case C) are listed in Table V. Compared with Table IV (Case B), the inductance of the Tx coil and NFC antenna are increased with the embedded ferrite sheet (Case C), which are almost the same as the inductance of Table III (Case A). Besides, the coupling coefficient between the Tx coil and NFC antenna is increased due to the embedded ferrite sheet. As for capacitances C_1, C_2, and C_M of Case C, they remain the same as Case B. Based on (2), (5), and (6), external capacitor C_{ext1} of 100 pF and C_{ext2} of 5.4 nF are used for compensation. With the load variation, the coil-to-coil efficiency and measured voltage V_{34} are indicated as blue curves in Fig. 25. Compared with Case B (red curve), the efficiency is significantly increased with the embedded ferrite (Case C). For example, with 20 Ω load resistance, the efficiency is enhanced from 74.28% (Case B) to 85.7% (Case C). Here, the small efficiency difference between Case A (89.25%) and Case C (85.7%) is mainly due to the additional loss on the ferrite and the components inside the smartphone. According to (15), the power transfer ratio for Case C is 2.95, which is smaller than Case B. Therefore, the measured V_{34} for Case C is bigger than that for Case B in Fig. 25(b). With 20 Ω load resistance, the experimental waveforms for Case C are depicted in Fig. 28. Compared with Fig. 26 (Case B), the distorted waveforms are restored to a certain extent. This is possibly because of the input impedance variation. With different input impedances, the output voltage waveform of the AG 1016 power amplifier will vary. Compared with the relatively small impedance of Case B, the input impedance of Case C is increased, which reduced the oscillation of input voltage V_1. The corresponding voltage V_{34} across the metal cover is 6.8 V, which meets the safety requirement.

In conclusion, the integrated smartphone will decrease the efficiency of the proposed coupler, which is mainly caused by the induced eddy current on the metallic components inside the smartphone. To fix this, a ferrite sheet can be embedded between the proposed coupler and the smartphone. Based on the

analyses above, the proposed coupler can be applied to practical smartphone applications.

VII. Conclusion

In this article, an NFC-CPT-connected coupler applying IPT-CPT-combined wireless charging is proposed for metal-cover smartphones. By converting the metal cover from a metal barrier to receiving plates, CPT through the metal cover is achieved. By connecting the inductive coils to the metal plates, the inductive coils perform as compensation inductance and power transfer coils simultaneously, thus realizing a combined IPT-CPT. Since the already-existing metal cover of 150 mm $\times$ 75 mm and NFC antenna of 30 mm $\times$ 22 mm are utilized to construct the receiver of the proposed coupler, only a parallel capacitor of 5 nF is integrated inside the smartphone, which greatly saves space and cost inside the smartphone. The power transfer ratio is set by adjusting the two external parallel capacitors C_{ext1} and C_{ext2} to be 100 pF and 5 nF, respectively. At 2.5 MHz operating frequency, 4.36 W inductive power and 1.75 W capacitive power are transferred with 89.25% coil-to-coil efficiency. With 5.6 W output power, the voltage across the metal cover is 7.08 V, which meets the safety voltage requirement at HF. By embedding a ferrite sheet, the proposed coupler can achieve 85.7% coil-to-coil efficiency and 5.32 V voltage across the metal cover with an actual smartphone attached. Considering space, cost, eddy current loss, and safety, the proposed NFC-connected coupler is a good candidate for metal-cover smartphone applications.

References

[1] S. Li and C. C. Mi, "Wireless power transfer for electric vehicle applications," *IEEE Trans. Emerg. Sel. Topics Power Electron.*, vol. 3, no. 1, pp. 4–17, Mar. 2015.

[2] S. Y. Hui, "Planar wireless charging technology for portable electronic products and Qi," *Proc. IEEE*, vol. 101, no. 6, pp. 1290–1301, Jun. 2013.

[3] "*The Qi wireless power transfer system power class 0 specification, parts 1 and 2: Interface definitions, ver. 1.2.3*," Wireless Power Consortium, Feb. 2017. [Online]. Available: https://www.wirelesspowerconsortium.com/data/downloadables/2/2/0/5/qi-wireless-power-specification-non-confidential.zip

[4] Y. Jang and M. Jovanovic, "A contactless electrical energy transmission system for portable-telephone battery chargers," *IEEE Trans. Ind. Electron.*, vol. 50, no. 3, pp. 520–527, Jun. 2003.

[5] C.-G. Kim, D.-H. Seo, J.-S. You, J.-H. Park, and B. H. Cho, "Design of a contactless battery charger for cellular phone," *IEEE Trans. Ind. Electron.*, vol. 48, no. 6, pp. 1238–1247, Dec. 2001.

[6] D. J. Graham, J. A. Neasham, and B. S. Sharif, "Investigation of methods for data communication and power delivery through metals," *IEEE Trans. Ind. Electron.*, vol. 58, no. 10, pp. 4972–4980, Oct. 2011.

[7] O. Imoru, A. Jassal, H. Polinder, E. Nieuwkoop, J. Tsado, and A. A. Jimoh, "An inductive power transfer through metal object," in *Proc. 1st Int. Future Energy Electron. Conf.*, Nov. 2013, pp. 246–251.

[8] J. Dai and D. Ludois, "A survey of wireless power transfer and a critical comparison of inductive and capacitive coupling for small gap applications," *IEEE Trans. Power Electron.*, vol. 30, no. 11, pp. 6017–6029, Nov. 2015.

[9] F. Lu, H. Zhang, H. Hofmann, and C. Mi, "A double-sided LCLC-compensated capacitive power transfer system for electric vehicle charging," *IEEE Trans. Power Electron.*, vol. 30, no. 11, pp. 6011–6014, Nov. 2015.

[10] H. Zhang, F. Lu, H. Hofmann, W. Liu, and C. Mi, "A four-plate compact capacitive coupler design and LCL-compensated topology for capacitive power transfer in electric vehicle charging application," *IEEE Trans. Power Electron.*, vol. 31, no. 12, pp. 8541–8551, Dec. 2016.

[11] *IEEE Standard for Safety Levels With Respect to Human Exposure to Radio Frequency Electromagnetic Fields, 3kHz to 300 GHz*, IEEE Std C95.1, 2005.

[12] *Method of Measurement of Touch Current and Protective Conductor Current*, IEC 60990, 1999.

[13] F. Lu, H. Zhang, and C. Mi, "A two-plate capacitive wireless power transfer system for electric vehicle charging applications," *IEEE Trans. Power Electron.*, vol. 33, no. 2, pp. 964–969, Feb. 2018.

[14] Y. Zhang, T. Kan, Z. Yan, Y. Mao, Z. Wu, and C. Mi, "Modeling and analysis of series-none compensation for wireless power transfer systems with a strong coupling," *IEEE Trans. Power Electron.*, vol. 34, no. 2, pp. 1209–1215, Feb. 2019.

[15] J. Kim, D. Kim, and Y. Park, "Analysis of capacitive impedance matching network for simultaneous wireless power transfer to multiple devices," *IEEE Trans. Ind. Electron.*, vol. 62, no. 5, pp. 2807–2813, May 2015.

[16] S. Li, W. Li, J. Deng, T. D. Nguyen, and C. Mi, "A double-sided LCC compensation network and its tuning method for wireless power transfer," *IEEE Trans. Veh. Technol.*, vol. 64, no. 6, pp. 2261–2273, Jun. 2015.

[17] J. Dai and D. C. Ludois, "Biologically inspired coupling pixilation for position independence in capacitive power transfer surfaces," in *Proc. IEEE Appl. Power Electron. Conf. Expo.*, 2015, pp. 3276–3282.

[18] L. Chao, A. P. Hu, G. A. Covic, and N. C. Nair, "Comparative study of CCPT systems with two different inductor tuning positions," *IEEE Trans. Power Electron.*, vol. 27, pp. 294–306, Jan. 2012.

[19] F. Lu, H. Zhang, H. Hofmann, and C. C. Mi, "A double-sided LC-Compensation circuit for loosely coupled capacitive power transfer," *IEEE Trans. Power Electron.*, vol. 33, no. 2, pp. 1633–1643, Feb. 2018.

[20] D. Vincent, P. S. Huynh, N. A. Azeez, L. Patnaik, and S. S. Williamson, "Evolution of hybrid inductive and capacitive AC links for wireless EV Charging—A comparative overview," *IEEE Trans. Transport. Electrific.*, vol. 5, no. 4, pp. 1060–1077, Dec. 2019.

[21] F. Lu, H. Zhang, H. Health, and C. C. Mi, "An inductive and capacitive combined wireless power transfer system with LC-compensated topology," *IEEE Trans. Power Electron.*, vol. 31, no. 12, pp. 8471–8482, Dec. 2016.

[22] B. Luo, T. Long, R. Mai, R. Dai, Z. He, and W. Li, "Analysis and design of hybrid inductive and capacitive wireless power transfer for high-power applications," *IET Power Electron.*, vol. 11, no. 14, pp. 2263–2270, Nov. 2018.

[23] F. Lu, H. Zhang, H. Hofmann, and C. C. Mi, "An inductive and capacitive integrated coupler and its LCL compensation circuit design for wireless power transfer," *IEEE Trans. Ind. Appl.*, vol. 53, no. 5, pp. 4903–4913, Sep./Oct. 2017.

[24] B. Luo, T. Long, L. Guo, R. Dai, R. Mai, and Z. He, "Analysis and design of inductive and capacitive hybrid wireless power transfer system for railway application," *IEEE Trans. Ind. Appl.*, vol. 56, no. 3, pp. 3034–3042, May/Jun. 2020.

[25] X. Li, C. Tang, X. Dai, P. Deng, and Y. Su, "An inductive and capacitive combined parallel transmission of power and data for wireless power transfer systems," *IEEE Trans. Power Electron.*, vol. 33, no. 6, pp. 4980–4991, Jun. 2018.

[26] Y. Su, W. Zhou, A. P. Hu, C. Tang, S. Xie, and Y. Sun, "Full-duplex communication on the shared channel of a capacitively coupled power transfer system," *IEEE Trans. Power Electron.*, vol. 32, no. 4, pp. 3229–3239, Apr. 2017.

[27] X. Y. Zhang, C.-D. Xue, and J.-K. Lin, "Distance-insensitive wireless power transfer using mixed electric and magnetic coupling for frequency splitting suppression," *IEEE Trans. Microw. Theory Techn.*, vol. 65, no. 11, pp. 4307–4316, Nov. 2017.

[28] W. Zhou, Y.-G. Su, L. Huang, X.-D. Qing, and A. P. Hu, "Wireless power transfer across a metal barrier by combined capacitive and inductive coupling," *IEEE Trans. Ind. Electron.*, vol. 66, no. 5, pp. 4031–4041, May 2019.

[29] J. Q. Zhu, Y. L. Ban, R. M. Xu, and C. C. Mi, "An NFC-CPT-combined coupler with series-none compensation for metal-cover smartphone applications," *IEEE J. Emerg. Sel. Topics Power Electron.*, early access, Jun. 16, 2020, doi: 10.1109/JESTPE.2020.3002858.

[30] J. Fischer, "NFC in cell phones: The new paradigm for an interactive world," *IEEE Commun. Mag.*, vol. 47, no. 6, pp. 22–28, Jun. 2009.

[31] Z. Yan *et al.*, "Frequency optimization of a loosely coupled underwater wireless power transfer system considering eddy current loss," *IEEE Trans. Ind. Electron.*, vol. 66, no. 5, pp. 3468–3476, May 2019.

[32] Y. Zhang, T. Lu, Z. Zhao, F. He, K. Chen, and L. Yuan, "Selective wireless power transfer to multiple loads using receivers of different resonant frequencies," *IEEE Trans. Power Electron.*, vol. 30, no. 11, pp. 6001–6005, Nov. 2015.

Jia-Qi Zhu was born in Henan, China, in 1992. He received the B.S. degree in electronic information science and technology from the Southwest Jiaotong University (SWJTU), Chengdu, China, in 2014. He is currently working toward the Ph.D. degree with the University of Electronic Science and Technology of China (UESTC), Chengdu, China.

In 2018, he received funding from UESTC and China Scholarship Council, and became a Joint Ph.D. Student with the Department of Electrical and Computer Engineering, San Diego State University, San Diego, CA, USA. His main research interests include near-field communication (NFC) and wireless power transfer (WPT) antennas for smartphone applications, especially near field antennas operating with metal-cover smartphones.

Yong-Ling Ban was born in Henan, China. He received the B.S. degree in mathematics from Shandong University, Jinan, China, in 2000, the M.S. degree in electromagnetics from Peking University, Beijing, China, in 2003, and the Ph.D. degree in microwave engineering from the University of Electronic Science and Technology of China (UESTC), Chengdu, China, in 2006, respectively.

In July 2006, he joined the Xi'an Mechanical and Electric Information Institute, Xi'an, China, as a Microwave Engineer. He then joined Huawei Technologies Co., Ltd., Shenzhen, China, where he designed and implemented various terminal antennas for 15 data card and mobile phone products customized from leading telecommunication industries such as Vodafone. From September 2010 to July 2016, he was an Associate Professor with UESTC, where he is currently a Professor. From May 2014 to April 2015, he visited Queen Mary University of London, as a Scholar Visitor. He is the author of more than 60 referred journal and conference papers on his research topics and holds 20 granted and pending Chinese and overseas patents. His research interests include wideband small antennas for 4G/5G handset devices, MIMO antennas, and millimeter wave antenna arrays.

Rui-Min Xu (Member, IEEE) was born in Sichuan, China, in 1958. He received the B.S. and Ph.D. degrees in electromagnetic field and microwave techniques from the University of Electronic Science and Technology of China (UESTC), Chengdu, China, in 1982 and 2007, respectively.

He is currently a Full Professor with UESTC. His current research interests include microwave and millimeter-wave technologies and applications, and radar systems.

Chunting Chris Mi (Fellow, IEEE) received the B.S.E.E. and M.S.E.E. degrees from the Northwestern Polytechnical University, Xi'an, China, in 1985 and 1988, respectively, and the Ph.D. degree from the University of Toronto, Toronto, ON, Canada, in 2001, all in electrical engineering.

He is currently a Professor and Chair of Electrical and Computer Engineering and the Director of the Department of Energy (DOE)-funded Graduate Automotive Technology Education (GATE) Center for Electric Drive Transportation, San Diego State University (SDSU), San Diego, CA, USA. Prior to joining SDSU, he was with University of Michigan-Dearborn, Dearborn, MI, USA, from 2001 to 2015.